DOI: 10.1002/ ((please add manuscript number))
Article type: Full Paper

Superior Lithium Storage Properties of β–FeOOH

Linghui Yu, Shibo Xi, Chao Wei, Wenyu Zhang, Yonghua Du, Qingyu Yan and Zhichuan J. Xu**

Dr. L. H. Yu, C, Wei, W. Y. Zhang, Prof. Q. Y. Yan, Prof. Z. C. Xu
School of Materials Science and Engineering, Nanyang Technological University, 50 Nanyang Avenue, 639798, Singapore
E-mail: xuzc@ntu.edu.sg
Dr. S. B. Xi, Dr. Y. H. Du
Institute of Chemical and Engineering Sciences, A*STAR, 1 Pesek Road, 627833，Singapore
E-mail: du_yonghua@ices.a-star.edu.sg
Prof. Z. C. Xu
Energy Research Institute @ NTU, Nanyang Technological University, 50 Nanyang Drive , 639798, Singapore

Keywords: lithium-ion batteries, anodes, β–FeOOH, porous electrodes

Several crystal forms of FeOOH were recently reported to be highly promising for lithium storage due to their high capacity, low cost and environmental friendliness. In particular, β–FeOOH has shown a capacity of ~1000 mAh g^{-1}, comparable to other promising iron-based anodes, such as Fe_2O_3 and Fe_3O_4. However, its storage mechanisms are unclear and the potential for further improvement remains unexplored. Here we show that this material can have a very high reversible capacity of ~1400 mAh g^{-1}, which is 20 – 40% higher than Fe_2O_3 and Fe_3O_4. Such a high capacity is delivered from a series of reactions including intercalation and conversion reactions, formation/de-formation of solid state electrolyte interface layers and interfacial storage. The mechanisms were studied by a combination of electrochemical and X-ray absorption near edge spectroscopic (XANES) approaches. Moreover, very long cycling performance, that is, after even more than 3000 cycles the material still has a significant capacity of more than 800 mAh g^{-1}, is obtained by a simple electrode design involving

introducing a rigid support into porous electrodes. Such long cycling performance is for the first time achieved for high-capacity materials based on conversion reactions.

1. Introduction

Due to the natural abundance and nontoxicity of iron, iron-based materials have always been attractive as electrodes for lithium-ion batteries (LIBs) which are the state-of-the-art energy storage technology today.[1] In this context, many iron oxides, such as Fe_2O_3 and Fe_3O_4, have been intensively studied as anodes for LIBs.[2] This is because these oxides can own a high capacity 1 to 2 times higher than that of commercial graphite anodes. Recently, several crystal structures of FeOOH, including α–, β– and amorphous forms, were reported to be highly promising as anodes for LIBs because of their high capacities that are comparable to Fe_2O_3 and Fe_3O_4.[3] However, similar to other high-capacity anode materials, these FeOOH materials usually suffer from fast capacity fading due to the instability of electrodes resulting from large volume change during lithiation/delithiation.[3e, 4] Therefore, advanced design of materials and/or electrodes is needed to improve their cyclability. So far, this still remains a great challenge. On the other hand, fundamental understanding of the lithium storage mechanisms of electrode materials is important for their developments in LIBs. However, research in this field for FeOOH materials is rather limited.

In particular, β–FeOOH for lithium storage was first reported by Amine et al. in 1999.[5] They investigated the lithium storage properties in a potential range of 1.5 – 4.3 V vs. Li^+/Li and demonstrated that ~1 lithium atom can reversibly intercalate/deintercalate into/from β–FeOOH per formula in this potential range, corresponding to the intercalation reaction: β–FeOOH + Li^+ + e^{-1}↔ LiFeOOH, where Fe(III) is reduced to Fe(II) during discharge and Fe(II) is re-oxidized to Fe(III) during charge. The theoretical capacity according to this reaction is 301.6 mAh g^{-1}. Because of the high capacity in the high potential range, this material was considered as a promising cathode for rechargeable lithium-metal batteries. In

their study, they also applied a low cut-off potential, 0.5 V vs. Li^+/Li, and a discharge capacity of ~1100 mAh g^{-1} was obtained. Following this work, there are several reports on β–FeOOH where it was also investigated in a high potential range.[6] The first study on β–FeOOH in a low potential range of 0.00 – 2.5 V vs. Li^+/Li was reported by Tabuchia et al in 2009.[3c] A high reversible capacity of ~1000 mAh g^{-1} was obtained in their study. Such a capacity is similar to those reported for Fe_2O_3 and Fe_3O_4 anodes, and much higher than the theoretical capacity of the commercial graphite of 372 mAh g^{-1}. They also proposed that surface reactions and partial reduction of Fe(II) to Fe(0) was responsible for the capacity in the low potential range. However, detailed storage mechanisms still remain unclear for capacity delivered below the potential of 1.5 V. Besides, the cycling performance reported was not satisfactory with showing only less than 20 cycles. Further improvement in performance remains unexplored.

Herein, we show that β–FeOOH could have a very high reversible capacity of ~1400 mAh g^{-1} in the potential range of 0.005 – 3 V vs. Li^+/Li, which is 20 – 40% higher than Fe_2O_3 and Fe_3O_4. Such a high capacity is delivered from a series of reactions including intercalation and conversion reactions, formation/de-formation of solid electrolyte interface (SEI) layers and interfacial storage. We discuss the reaction mechanisms by a combination of electrochemical and X-ray absorption near edge spectroscopic (XANES) studies. Moreover, by a simple design of electrode, we obtain very long cycling performance, that is, after even more than 3000 cycles the material still has a significant capacity of more than 800 mAh g^{-1}. Such long cycling performance is for the first time achieved for high-capacity materials based on conversion or alloying reactions.

2. Results and Discussion

β–FeOOH was prepared by a simple hydrolysis process at 100 °C using $FeCl_3$ as a precursor. Scanning electron microscopy (SEM) image (**Figure 1**a) shows that the product owns a rod-

like structure with a diameter of ~100 nm. The X-ray diffraction (XRD) pattern (Figure 1b) confirms the single-phase character of the product that all the peaks can be indexed into tetragonal β–FeOOH (JCPDS card No.: 34-1266).

Figure 2a shows the first five discharge/charge curves of the β–FeOOH electrode containing 15% SP carbon at a current density of 0.2 A g^{-1}. The electrode has initial discharge and charge capacities of 1759 and 1424 mAh g^{-1}, respectively. The capacity of the electrodes was always calculated based on the mass of β–FeOOH in this work unless otherwise stated. The SP carbon electrode without β–FeOOH was also tested as reference (**Figure S1**). Only a small contribution of the capacity is from SP carbon, ~ 105 and 58 mAh g^{-1} for discharge and charge, respectively. Thus, the reversible (discharge) capacity that originates from β–FeOOH is ~ 1366 mAh g^{-1}. This is much higher than the previous report of ~1000 mAh g^{-1} and also 20 – 40 % higher than those widely reported for Fe_2O_3 and Fe_3O_4 anodes.[2a-e, 3g, 7] Such a high capacity makes it very competitive with Fe_2O_3 or Fe_3O_4 anodes.

To understand how the capacity is delivered, we acquired more information from our results. As can be seen from Figure 2a, the first discharge curve is composed of four plateaus and sloping regions, indicating a multiple-step process of lithiation. The first sloping voltage plateau is observed around 1.85 V which is attributed to lithium intercalation into β–FeOOH to form LiFeOOH. The theoretical capacity of this intercalation step is 301.6 mAh g^{-1}. In previous reports, a capacity of larger than 270 mAh g^{-1} could be obtained when discharged to 1.5 V at low current densities.[5-6, 8] Here, at this potential, the capacity for the electrode is 243 mAh g^{-1}(a capacity of less than 1 mAh g^{-1} from the SP carbon; see **Table S1** for capacities of the SP carbon at different potentials), corresponding to $Li_{0.80}FeOOH$, and lower than literature data. This might be due to different current densities applied as well as lower utilization of the material. In our case, it's more likely that this intercalation reaction ends at a slightly lower potential.

Following the first intercalation reaction, there is a second sloping region which ends at ~ 0.93 V. The capacity for the electrode at this potential is 564 mAh g^{-1} including a contribution of ~17 mAh g^{-1} from the SP carbon, corresponding to $Li_{1.82}FeOOH$, which is very close to uptake of two lithium per β–FeOOH with a theoretical capacity of 603.3 mAh g^{-1}. This means after the first intercalation reaction, about one more lithium intercalate into β–FeOOH. The valence of iron after this reaction is likely to be reduced to be close to Fe(I) according the capacity. However, it should be noted that it's also reported the formation of solid electrolyte interface (SEI) layers could start at this region and contribute a certain capacity.[3c, 9]

After the sloping region, a long and flat voltage plateau is found ending at ~0.65 V. This is attributed to: (1) a conversion reaction to form metallic iron, Fe(0), as will be discussed later; and (2) formation of solid electrolyte interface (SEI) layers. The capacity for the electrode at 0.65 V is 1307 mAh g^{-1} including a contribution of ~31 mAh g^{-1} from the SP carbon. The theoretical capacity of β–FeOOH from Fe(III) to Fe(0) is 905 mAh g^{-1}. Thus the capacity from the formation of the SEI layers at this stage is larger than 371 mAh g^{-1} by excluding the theoretical capacity from Fe(III) to Fe(0) and the contribution from SP. The following sloping region after the conversion plateau could be partially due to further formation of SEI layers. Besides, interfacial storage with a capacitive character probably is also contribute to the capacity in this region because such a storage behavior generally exists in low potentials for materials based on conversion reactions.[4b] The final discharge capacity for the electrode is 1759 mAh g^{-1} at a cut-off potential of 0.005 V as mentioned before.

In the subsequent charging process, the profile is composed of two sloping regions in the low and high potential ranges, and two less defined plateaus (~0.95 – ~1.3 V and ~1.3 – ~2.2 V) in-between. Such a characteristic of the profile also indicates multiple-step reactions, probably including interfacial storage, de-formation/consumption of SEI layer, and conversion and intercalation reactions. The capacity attained during this process is 1424 mAh g^{-1} as mentioned before, corresponding to an irreversible capacity of 336 mAh g^{-1} and a

coulombic efficiency of 81% for the first cycle. The observation of the irreversible capacity indicates some of the reactions mentioned above are irreversible or partially irreversible. The coulombic efficiency of 81% could probably be further improved by charging to a higher potential because at least the first intercalation reaction is more reversible in a higher potential range, e.g. 1.5 – 4.3 V.[5]

For the second cycle, it is observed that the shape of the discharge profile above 0.93 V is different from the first, with the absence of the first intercalation plateau. The capacity of the electrode at this potential is also much lower for the second discharge, only 76.6 % of the first one. These indicate the poor reversibility of the reactions occurring above 0.93 V. The capacity reduces fast every cycle during the first five cycles, indicating the instability of the electrode which will be further discussed later.

The discharge/charge processes were monitored by XRD to determine the phase structure of the lithiation/delithiation products, as shown in **Figure S2**. It is found that the material loses its crystallinity even just at 1.5 V during the 1st discharge. And it remains amorphous in the following discharge and charge processes. The amorphous feature of the de-conversion products is consistent with other materials based on conversion reactions.[4b]

Cyclic voltammetry (CV) was also employed to investigate the lithiation/delithiation behavior of the β–FeOOH. As can be seen from Figure 2b, the first negative scan is characterized by four peaks centered at 1.78, 1.25, 0.73 and ~0 V, corresponding to the four regions in the first discharge profile from high to low potentials, respectively. In the subsequent positive scan, a well-defined peak is first obtained centered at 1.04 V corresponding to the region between ~0.95 – ~1.3 V in the first charge profile. A second broad peak is then observed centered at 1.55 V probably corresponding to the de-conversion reaction. Following these two peaks, there are two other shoulder peaks which are almost undistinguishable, at 1.96 and 2.19 V. These two peaks may be attributed to the reversible reactions corresponding to the cathodic peaks at 1.25 and 1.78 V, respectively. They overlap

with each other and with the broad peak around 1.55 V in some degree, indicating that these reactions take place at the same time at certain potential range.

In the following cycle, we can see all the peaks become less pronounced compared with the first cycle except the most pronounced cathodic peak at 0.75 V. This indicates that the conversion reaction and formation of SEI layers at this potential are highly reversible and that the other reactions are partially reversible. Besides, it is found that the first three cathodic peakes shifted to higher potentials during the second cycle, i.e., 1.78 →1.85 V, 1.24 → 1.43 V and 0.73 → 0.75 V, indicating lower polarization, in agreement with the discharge/charge profiles that the initial sloping regions and the conversion plateau for the second cycle locate at slightly higher potentials than for the first cycle. The anodic peak at 1.82 V in the second cycle could be due to further overlap of the reactions occurring at 1.96 and 2.19 V in the first cycle.

To further understand the lithiation/delithiation behavior of β–FeOOH, we performed XANES analysis on the β–FeOOH electrodes at different discharge and charge states during the first two cycles. The XANES spectra are shown in **Figure 3**a-f. Their first derivative plots are shown in **Figure S3**. The states chosen for this study are shown in Figure 3g. From the XANES spectra, we can obtain the valence information of the iron because the overall iron absorption edge position will shift to lower energies with reducing the average oxidation state of iron due to the decrease in binding energy of the Fe $1s^2$ electrons. [10] The β–FeOOH (fresh electrode) and reference Fe_2O_3 have the same absorption edge position on the spectra (Figure 3f) because of the same oxidization state of iron. With discharge to 1.5, 0.93, and 0.65 V, the edge position shifts to lower energy continuously, and then remains the same till 0.005 V, indicating a continuous reduction of iron till 0.65 V and no obvious reduction of iron upon further discharge. It is well known that there is a conversion reaction during electrochemical lithiation for many transition metal oxides, after which the transition metallic element is reduced to its elemental state. It was also reported that there is a similar conversion reaction

for α–FeOOH to form Fe(0), LiOH and Li_2O.[3f] Thus, it's interesting to know if there is also such a conversion reaction for β–FeOOH. This point can be confirmed by comparing the XANES spectra of the sample and metallic iron reference. As shown in Figure 3f, the absorption edge of the spectrum after discharge to 0.65 V is close to the iron reference; the main peak positions of the first derivative plot (Figure S3f) for the sample are consistent with those of the iron reference. These suggest the formation of Fe(0), and thus confirming the presence of a conversion reaction. The signal vibration amplitude of the sample is smaller than that of the iron reference, indicating that the iron tends to be amorphous in the sample. Combining with the electrochemical results above, we may conclude that Fe(III) in β–FeOOH is firstly reduced to Fe(II) by an intercalation reaction which ends at ~1.5 V; and then reduced to Fe(x) by another intercalation reaction which ends at ~0.93 V (x may be close to 1 if assuming the capacity contribution from the formation of SEI layers is low at this relatively high potential range); and finally reduced to Fe(0) by a conversion reaction which ends at ~0.65 V, probably coupled with the formation of LiOH and Li_2O as proposed for α-FeOOH. For the further discharge process to 0.005 V, the iron is not involved in the redox reactions. This is consistent with other reports[4b] for conversion materials that the capacity at low potential ranges comes from decomposition of electrolytes to form SEI layers and interfacial storage, because the redox center (here iron) in the materials has been completely reduced to the lowest valence state after conversion reactions.

Figure 3b shows the Fe K-edge XANES spectra of the electrodes recharged to 0.95, 1.3, 2.2, and 3 V after discharge to 0.005 V comparing with the 0.005 V one. It's interestingly found that the curves for 0.005, 0.95, and 1.3 V almost overlap with each other, indicating the same valence state of iron till 1.3 V. This suggests that the capacity below 1.3 V is because of de-formation of SEI layers and/or interfacial storage, and oxidation of Fe is not involved. However, we can notice that the first charge profile (Figure 2a) shows two distinguishable regions (0.95 – 1.3 V and <0.95V) in the low potential range, indicating different mechanisms

involved. This point needs to be further studied by other techniques. Upon further charge to higher potential, the valence state of the iron continuously increases as evidenced by the shift of the Fe absorption edge position to higher energy. However, the final valence (3 V) is still lower than the initial one but close to the 1.5 V (1st discharge) one (Figure 3e), i.e., the average oxidation state at 3 V is slightly higher than Fe(II) because the lithiation state at 1.5 V(1st discharge) is $Li_{0.80}FeOOH$ in our case. This indicates the irreversibility of the reactions, in agreement with the electrochemical results.

The Fe K-edge XANES spectra for the following cycle show the same trend for the valence change of iron (Figure 3c and d). Namely, the iron is reduced continuously until completion of conversion reaction (~0.65 V) and then remains Fe(0) till 0.005 V during discharge. Upon charge, oxidation of iron starts above 1.3 V, and the final valence (3.0 V) of the iron is also close to the 1.5 V (1st discharge) one. For better comparison of the oxidation state at low potentials, we combined all the spectra and their first derivatives for the ones after the conversion reaction and before oxidation of iron in the same figure (**Figure S4**), and it is observed that all these curves almost overlap with each other, which means that they have the same oxidation state.

Based on the discussion above, we thus propose such mechanisms for lithium storage in β–FeOOH including the following reactions:

(1) β–Fe(III)OOH + $Li^+ + e^{-1}$ ↔ LiFe(II)OOH (partially reversible)

(2) LiFe(II)OOH + $xLi^+ + xe^{-1}$ ↔ Li_{1+x}Fe(II-x)OOH (partially reversible)

(3) Li_{1+x}Fe(II-x)OOH + $(2-x)Li^+ + (2-x)e^{-1}$ ↔ Fe(0) + Li_2O + LiOH (highly reversible)

(4) Formation and de-formation of SEI layers and interfacial storage (partially reversible)

The rate and cycling properties of the material are shown in **Figure 4**a (the one without graphite). Initially, the capacity decreases fast every cycle, and a reversible capacity of 806

mAh g^{-1} for the electrode at a current density of 0.2 A g^{-1} is obtained after 5 cycles, corresponding to a retention of 57%. The fast capacity fading should be mainly because of the instability caused by large volume change during lithiation/delithiation which is always associated with high-capacity conversion and alloying materials. Besides, as mentioned above, the low voltage range applied also accounts for partial irreversible capacity because at least the first intercalation reaction is more reversible in a higher voltage range as reported. The stability of the electrode was also investigated by SEM. **Figure S5**a and b show the SEM images of the electrodes before and after one cycle, respectively. It is observed that the electrode becomes seriously cracked after one cycle (Figure S5b) as compared with the fresh electrode (Figure S5a). The cracking leads to the loss of electrical contact of the electrode. This confirms the instable nature of the electrode during lithiation and delithiation. Moreover, the high magnification image of the electrode after one cycle (Figure S5d) shows the absence of the original rod-like particles. Note that our electrode processing technique didn't destroy the rod-like structure as confirmed by the high magnification images of the fresh electrode (Figure S5c). Instead, we only observe the agglomerates of small nanoparticles. This is consistent with those widely reported that the cracking of the electrode is accompanied with agglomeration.[11] The formation of nanoparticles after cycling is also commonly reported for materials that undergo a conversion reaction.[4b, 12]

In the next 30 cycles, the current density was increased every 10 cycles from 0.5 A g^{-1} to 1 A g^{-1}, and then 2 A g^{-1} for rate capability measurement. The capacity gradually decreases at each rate. The reversible capacities for the electrode are 576, 399, and 254 mAh g^{-1} at 10^{th} (0.5 A g^{-1}), 20^{th} (1 A g^{-1}), and 30^{th} (2 A g^{-1}) cycle, respectively. Afterward, the battery was cycled at a current density of 0.5 A g^{-1}. The capacity still keeps decreasing in the following tens of cycles. And after reaching to the lowest point of 285 mAh g^{-1} at this rate, the capacity starts increasing gradually. After ~300 cycles totally, the capacity for the electrode maintains between 500 and 600 mAh g^{-1} for the next 300 hundreds of cycles. The instable cycling

behavior in the first 300 cycles is ascribed to a restructuring process of the electrode.[2d, 13] Firstly, the large volume change results in the capacity fading in these initial cycles. As the cycling proceeds, the SEI layers, which is able to alleviate the volume swing,[2d] formed on the surface of the particles might become more and more stable. Moreover, it might be possible for the electrical contact to recover in some degree upon cycling because the electrode undergoes an aggregation process during discharge/charge. These lead to the increase of the capacity until final stabilization. Similar restructuring behavior has been also found for other high-capacity materials.[2d, 3e, 4g] Here, our result shows that this restructuring process may take several hundreds of cycles for the electrode to reach a stable state.

In order to improve the cycling performance, it is necessary to design a stable electrode that can accommodate the volume change during lithiation and delithiation. An ideal electrode for large-volume-change materials should contain pre-reserved spaces for volume expansions and have a rigid component to maintain the whole structure.[4h, 14] As reported, materials with nanorod-like structures are always highly porous, because they own pores generated between the rods when randomly stacking together. [15] These pores can ideally serve as spaces for volume expansions. The porosity of our β–FeOOH was also confirmed by N_2 adsorption measurement. The isotherm (**Figure S6**) shows a typical type Ⅳ profile with an obvious capillary condensation, indicative of mesoporosity of the material. The BJH pore volume and BET surface area are 0.22 cm^3 g^{-1} and 16 m^2 g^{-1}, respectively. To improve the stability of the electrode, we introduced microsized sheet-like graphite (**Figure S7**a) into the electrode as a rigid support. The use of graphite to improve cycling performance has been reported before.[16] Here we show that by combining the sheet-like graphite and porous electrode materials, very long cycling performance could be achieved.

Partial (10 wt% in the electrode) of the SP carbon which was used as a conductive additive in the electrode was first replaced with the same amount of graphite. The cycling and rate properties for this electrode are also shown in Figure 4. The first and fifth reversible

capacities for the electrode are 1268 and 907 mAh g^{-1} at a current rate of 0.2 A g^{-1}, corresponding to a retention of 72%, which is much higher than the one without graphite. Besides, although this electrode doesn't show improvement in rate capability, it has a higher capacity after rate capability testing. These facts prove the efficient improvement of stability by using graphite.

To further enhance the stability, a higher content of graphite was used in the electrode (30 wt%) and the use of β–FeOOH was correspondingly reduced to 50 wt% from 70 wt%. The cycling and rate properties for this electrode are shown in **Figure 5**. The first reversible capacity for the electrode increases to 1564 mAh g^{-1} at a current density of 0.2 A g^{-1} because of a large contribution from the high-content graphite (see Figure S7b for the capacity of the graphite electrode). After 5 cycles at the same rate, the capacity for the electrode reduces to 1338 mAh g^{-1} corresponding to a retention of 86%, which is further improvement to the electrode with 10 % of graphite. To gain insight into the improvement, SEM was used to investigate the structure of the electrodes with 30 wt% of graphite before (Figure S5e) and after cycling (Figure S8f and g). From the SEM image of the one after one cycle (Figure S5f), we can see only slight cracking. And after two cycles (Figure S5g), the cracking is still rather moderate compared with the one without graphite after one cycle (Figure S5b). These observations demonstrate that the use of graphite is favorable for the maintenance of the mechanical integrity of the electrode.

For the next 30 cycles, the current densities applied were the same as the electrode without graphite for comparison. Due to the improved stability, the capacities become rather stable at each rate without any visible fading. Besides, the rate capability is also improved, with a reversible capacity of 1216, 1131, and 1017 mAh g^{-1} at 10^{th} (0.5 A g^{-1}), 20^{th} (1 A g^{-1}), and 30^{th} (2 A g^{-1}) cycle for the electrode. The current density was further increased to 5 A g^{-1} and 10 A g^{-1} for the 36 – 45^{th} and 46 – 55^{th} cycles. A very high capacity of 684 mAh g^{-1} (50^{th}) is still retained at 10 A g^{-1}, corresponding to ~4 min charging/discharging. Both the improved

stability and conductivity by adding the high content graphite should be account for this excellent rate capability. It's worth to note that graphite is not capable of fast intercalation/de-intercalation of lithium (68 and 34 mAh g^{-1} at a current density of 1 and 2 A g^{-1}, respectively, Figure S7b). Therefore, it has negligible contribution to capacity at high rates.

From 55th to 3000th cycle, the battery was cycled at a current density of 2 A g^{-1}. The capacity for the electrode undergoes firstly a gradually increase even up to 1605 mAh g^{-1} (337th) and then decrease till stabilized at ~ 600 mAh g^{-1}, indicating also a restructuring process. After 3000 cycles, the current density was reduced to 0.5 A g^{-1} and a capacity of up to 1048 mAh g^{-1} for the electrode could still be obtained for the electrode. Note that the capacity contribution from the graphite and the SP carbon should be less that 222 mAh g^{-1} (calculated based on the capacity of 370 mAh g^{-1} for the graphite electrode at a low current density of 50 mAh g^{-1}). This means the β–FeOOH still have more than 800 mAh g^{-1} after 3000 cycles. To the best of our knowledge, such long cycling performance has never been achieved for any materials based on conversion reactions. A disadvantage here is the use of a high content of graphite with a lower capacity which compromises the overall specific capacity of the electrode. However, such a compromise would be acceptable because it's also common to use carbon composites with high carbon content, e.g., 20 – 40 %, for large-volume-change electrode materials. [3e, 4f, 4h, 14b, 17]

3. Conclusion

We reported here a large reversible capacity of ~1400 mAh g^{-1} for β–FeOOH as anodes for LIBs. Such a capacity is much higher than the previous report of ~1000 mAh g^{-1} and also 20 – 40 % higher than those widely reported for other promising Fe_2O_3 and Fe_3O_4 anodes. By a combination of electrochemical and XANES studies, we proposed the lithium storage mechanisms for β–FeOOH, including the following reactions:

(1) β–Fe(III)OOH + Li^+ + e^{-1} ↔ LiFe(II)OOH (partially reversible)

(2) $LiFe(II)OOH + xLi^{+} + xe^{-1} \leftrightarrow Li_{1+x}Fe(II\ -x)OOH$ (partially reversible)

(3) $Li_{1+x}Fe(II\ -x)OOH + (2-x)Li^{+} + (2-x)e^{-1} \leftrightarrow Fe(0) + Li_2O + LiOH$ (highly reversible)

(4) Formation and de-formation of SEI layers and interfacial storage (partially reversible)

Moreover, very long cycling performance, which has never been achieved for any conversion materials, were obtained by a simple electrode design using microsized sheet-like graphite as a rigid support and self-generated pores between nanorods as pre-reserved spaces for the volume change. This simple approach to a more stable electrode would be also applicable to other high-volume-change conversion and alloying materials.

4. Experimental Section

Synthesis of β–FeOOH. β–FeOOH was synthesized by a hydrolysis method. In a typical synthesis, 10 mL of 0.5 M aqueous $FeCl_3$ was added into 70 mL of H_2O in a 100 mL plastic bottle with a 0.8 mm needle hole. After shaking for 1 – 2 min, the bottle was kept in an oven at 100 °C for 24 h. The precipitates were collected after cooling down and washed with deionized water and ethanol several times and finally dried at 80 °C overnight.

Characterization. X-ray powder diffraction (XRD) analysis of the samples were carried out with a Shimadzu thin film diffractometer using Cu Kα radiation. Field-Emission Scanning electron microscopy (FESEM) images were collected on JEOL JSM-6340F and 7600F microscopes. High-resolution transmission electron microscopy (HRTEM) images were observed using a JEOL JEM 2010 microscope. Nitrogen adsorption measurements were performed on a Micromeritics ASAP 2020 physisorption analyzer at 77 K. Brunauer−Emmett−Teller (BET) and Barret-Joyner-Halenda (BJH) methods were used for the surface area and pore size distribution (PSD) determination using N_2 adsorption data. X-ray absorption near edge spectroscopy (XANES) was carried out at Singapore Synchrotron Light Source, XAFCA beamline.

Electrochemical Measurements. The active material β–FeOOH nanorods were mixed with conductive carbon (Super P, SP) and binder (sodium carboxymethyl cellulose, CMC) in deionized water in a weight ratio of 70 : 15 : 15. The resultant slurry was coated onto a current collector and dried at 80 °C overnight. To improve the cycling performance, graphite was added into the electrodes. Two weight ratios of β–FeOOH : graphite : SP : CMC were used, 70 : 10 : 5 : 15 and 50 : 30 : 5 : 15. The loading density of the electrodes was ~ 1 mg cm^{-2}. Due to the different composition of electrodes, all the capacities and current densities in this work were normalized by the mass of β–FeOOH unless otherwise stated. The electrodes were assembled with Li metal as counter electrodes in a 2032 coin cell in an Ar-filled glove box. Celgard 2400 was used as a separator. The electrolyte was 1 M $LiPF_6$ in ethylene carbonate/dimethyl carbonate (1/1 by volume). Galvanostatic charge and discharge (0.005 – 3 V) tests were performed on Battery Testing Equipment (Neware Electronic Co., China) at different current densities under ambient temperature. Cyclic voltammetry measurement was performed on a Bio-Logic SP-150 potentiostat.

Supporting Information
Supporting Information is available from the Wiley Online Library or from the author.

Acknowledgements
This work was supported by MOE Tier 1 Grant (RGT13/13) of Singapore and the Singapore National Research Foundation under its Campus for Research Excellence And Technological Enterprise (CREATE) programme. Authors thank the facility support provided by the Singapore Synchrotron Light Source.

Received: ((will be filled in by the editorial staff))
Revised: ((will be filled in by the editorial staff))
Published online: ((will be filled in by the editorial staff))

[1] a) M. Wagemaker, F. M. Mulder, *Acc. Chem. Res.* **2013**, *46*, 1206; b) J. B. Goodenough, K.-S. Park, *J. Am. Chem. Soc.* **2013**, *135*, 1167; c) U. N. Maiti, W. J. Lee, J. M. Lee, Y. Oh, J. Y. Kim, J. E. Kim, J. Shim, T. H. Han, S. O. Kim, *Adv. Mater.* **2014**, *26*, 40.

[2] a) L. Taberna, S. Mitra, P. Poizot, P. Simon, J. M. Tarascon, *Nat. Mater.* **2006**, *5*, 567; b) M. V. Reddy, T. Yu, C. H. Sow, Z. X. Shen, C. T. Lim, G. V. S. Rao, B. V. R. Chowdari, *Adv. Funct. Mater.* **2007**, *17*, 2792; c) P. C. Lian, X. F. Zhu, H. F. Xiang, Z. Li, W. S. Yang, H. H. Wang, *Electrochim. Acta* **2010**, *56*, 834; d) J. Zhu, Z. Yin, D. Yang, T. Sun, H. Yu, H. E. Hoster, H. H. Hng, H. Zhang, Q. Yan, *Energy Environ. Sci.* **2013**, *6*, 987; e) B. B. Tian, J. Swiatowska, V. Maurice, S. Zanna, A. Seyeux, L. H. Klein, P. Marcus, *Langmuir* **2014**, *30*, 3538; f) F. Y. Cheng, J. Liang, Z. L. Tao, J. Chen, *Adv. Mater.* **2011**, *23*, 1695; g) W. J. Lee, U. N. Maiti, J. M. Lee, J. Lim, T. H. Han, S. O. Kim, *Chem. Commun.* **2014**, *50*, 6818.

[3] a) J. Wang, L. Li, C. L. Wong, L. Sun, Z. Shen, S. Madhavi, *Rsc Advances* **2013**, *3*, 15316; b) C. Zhang, J. Zhu, X. Rui, J. Chen, D. Sim, W. Shi, H. H. Hng, T. M. Lim, Q. Yan, *CrystEngComm* **2012**, *14*, 147; c) T. Tabuchi, Y. Katayama, T. Nukuda, Z. Ogumi, *J. Power Sources* **2009**, *191*, 636; d) C. Xu, Y. Zeng, X. Rui, J. Zhu, H. Tan, A. Guerrero, J. Toribio, J. Bisquert, G. Garcia-Belmonte, Q. Yan, *J. Phys. Chem. C* **2013**, *117*, 17462; e) Y. Sun, X. Hu, W. Luo, H. Xu, C. Hu, Y. Huang, *ACS Appl. Mater. Interfaces* **2013**, *5*, 10145; f) X. Lou, X. Wu, Y. Zhang, *Electrochem. Commun.* **2009**, *11*, 1696; g) L. Zhang, H. B. Wu, X. W. Lou, *Adv. Energy Mater.* **2014**, *4*; h) J. S. Luo, X. H. Xia, Y. S. Luo, C. Guan, J. L. Liu, X. Y. Qi, C. F. Ng, T. Yu, H. Zhang, H. J. Fan, *Adv. Energy Mater.* **2013**, *3*, 737.

[4] a) M. M. Thackeray, C. Wolverton, E. D. Isaacs, *Energy Environ. Sci.* **2012**, *5*, 7854; b) J. Cabana, L. Monconduit, D. Larcher, M. Rosa Palacin, *Adv. Mater.* **2010**, *22*, E170; c) Y.-S. Hu, R. Demir-Cakan, M.-M. Titirici, J.-O. Müller, R. Schlögl, M. Antonietti, J. Maier, *Angew. Chem.* **2008**, *120*, 1669; d) Y. S. Hu, R. Demir-Cakan, M. M. Titirici, J. O. Muller, R. Schlogl, M. Antonietti, J. Maier, *Angew. Chem. Int. Ed.* **2008**, *47*, 1645; e) R. Demir-Cakan, Y. S. Hu, M. Antonietti, J. Maier, M. M. Titirici, *Chem. Mater.* **2008**, *20*, 1227; f) S. Liang, X. Zhu, P. Lian, W. Yang, H. Wang, *J. Solid State Chem.* **2011**, *184*, 1400; g) P. Lian, X. Zhu, S. Liang, Z. Li, W. Yang, H. Wang, *Electrochim. Acta* **2011**, *56*, 4532; h) X. W. Lou, C. M. Li, L. A. Archer, *Adv. Mater.* **2009**, *21*, 2536; i) D. D. Li, L. X. Ding, S. Q. Wang, D. D. Cai, H.

H. Wang, *J. Mater. Chem. A,* **2014**, *2*, 5625; j) W. J. Lee, T. H. Hwang, J. O. Hwang, H. W. Kim, J. Lim, H. Y. Jeong, J. Shim, T. H. Han, J. Y. Kim, J. W. Choi, S. O. Kim, *Energy Environ. Sci.* **2014**, *7*, 621.

[5] K. Amine, H. Yasuda, M. Yamachi, *J. Power Sources* **1999**, *82*, 221.

[6] a) X. Wang, X. Y. Chen, L. S. Gao, H. G. Zheng, M. R. Ji, C. M. Tang, T. Shen, Z. D. Zhang, *J. Mater. Chem.* **2004**, *14*, 905; b) T. Tabuchi, Y. Katayama, T. Nukuda, Z. Ogumi, *J. Power Sources* **2009**, *191*, 640; c) A. Funabiki, H. Yasuda, M. Yamachi, *J. Power Sources* **2003**, *119*, 290; d) Y. Fujino, T. Tabuchi, H. Yasuda, M. Yamachi, **2005**; e) C. Benoit, C. Bourbon, P. Berthet, S. Franger, *J. Phys. Chem. Solids* **2006**, *67*, 1265.

[7] W. M. Zhang, X. L. Wu, J. S. Hu, Y. G. Guo, L. J. Wan, *Adv. Funct. Mater.* **2008**, *18*, 3941.

[8] H. F. Shao, X. F. Qian, J. Yin, Z. K. Zhu, *J. Solid State Chem.* **2005**, *178*, 3130.

[9] B. B. Tian, J. Swiatowska, V. Maurice, S. Zanna, A. Seyeux, L. H. Klein, P. Marcus, *J. Phys. Chem. C* **2013**, *117*, 21651.

[10] a) O. Haas, A. Deb, E. J. Cairns, A. Wokaun, *J. Electrochem. Soc.* **2005**, *152*, A191; b) Z. Shadike, Y. N. Zhou, F. Ding, L. Sang, K. W. Nam, X. Q. Yang, Z. W. Fu, *J. Power Sources* **2014**, *260*, 72; c) T. Nedoseykina, M. G. Kim, S. A. Park, H. S. Kim, S. B. Kim, J. Cho, Y. Lee, *Electrochim. Acta* **2010**, *55*, 8876; d) S. Kostov, M. denBoer, E. Strauss, D. Golodnitsky, S. G. Greenbaum, E. Peled, *J. Power Sources* **1999**, *81–82*, 709; e) S. A. Wilson, E. Green, Mathews, II, M. Benfatto, K. O. Hodgson, B. Hedman, R. Sarangi, *Proc. Natl. Acad. Sci. U. S. A.* **2013**, *110*, 16333; f) A. J. Berry, H. S. O'Neill, K. D. Jayasuriya, S. J. Campbell, G. J. Foran, *Am. Mineral.* **2003**, *88*, 967.

[11] a) G. Zhou, D.-W. Wang, F. Li, L. Zhang, N. Li, Z.-S. Wu, L. Wen, G. Q. Lu, H.-M. Cheng, *Chem. Mater.* **2010**, *22*, 5306; b) M. Winter, J. O. Besenhard, M. E. Spahr, P. Novak, *Adv. Mater.* **1998**, *10*, 725.

[12] P. Poizot, S. Laruelle, S. Grugeon, L. Dupont, J. M. Tarascon, *Nature* **2000**, *407*, 496.

[13] G. Derrien, J. Hassoun, S. Panero, B. Scrosati, *Adv. Mater.* **2007**, *19*, 2336.

[14] a) W. M. Zhang, J. S. Hu, Y. G. Guo, S. F. Zheng, L. S. Zhong, W. G. Song, L. J. Wan, *Adv. Mater.* **2008**, *20*, 1160; b) N. Liu, Z. D. Lu, J. Zhao, M. T. McDowell, H. W. Lee, W. T. Zhao, Y. Cui, *Nat. Nanotechnol.* **2014**, *9*, 187; c) A. Magasinski, P. Dixon, B. Hertzberg, A. Kvit, J. Ayala, G. Yushin, *Nat. Mater.* **2010**, *9*, 353.

[15] a) L. H. Yu, D. D. Cai, H. H. Wang, M. M. Titirici, *Rsc Advances* **2013**, *3*, 17281; b) Z. Y. Yuan, B. L. Su, *Chem. Phys. Lett.* **2003**, *381*, 710.

[16] M. Nagayama, T. Morita, H. Ikuta, M. Wakihara, M. Takano, S. Kawasaki, *Solid State Ionics* **1998**, *106*, 33.

[17] a) X. W. Lou, D. Deng, J. Y. Lee, L. A. Archer, *Chem. Mater.* **2008**, *20*, 6562; b) Y. Qiu, K. Yan, S. Yang, *Chem. Commun.* **2010**, *46*, 8359; c) Y. Yu, L. Gu, C. Zhu, P. A. van Aken, J. Maier, *J. Am. Chem. Soc.* **2009**, *131*, 15984; d) Z. Zhang, Y. Wang, W. Ren, Q. Tan, Y. Chen, H. Li, Z. Zhong, F. Su, *Angew. Chem. Int. Ed.* **2014**, *53*, 5165; e) Z. Zhang, Y. Wang, W. Ren, Q. Tan, Y. Chen, H. Li, Z. Zhong, F. Su, *Angew. Chem.* **2014**, *126*, 5265.

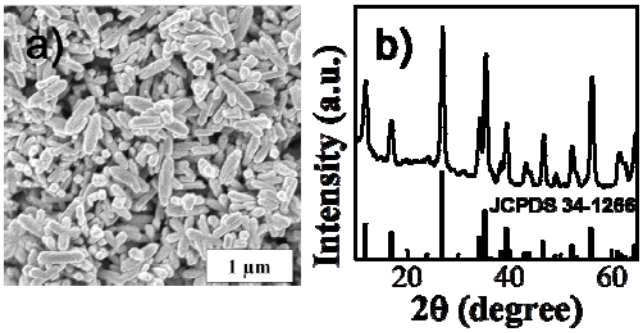

Figure 1. a) XRD pattern and b) SEM image of the prepared β–FeOOH

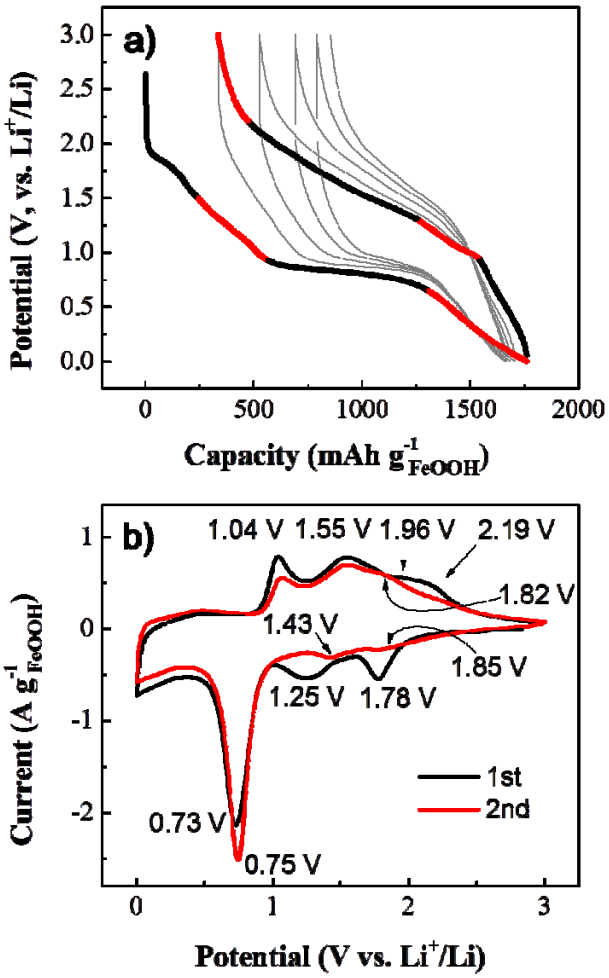

Figure 2. a) First five discharge/charge curve of the β–FeOOH at a current density of 0.2 A g^{-1}. Electrode components: 70 wt% β–FeOOH-1 / 15 wt% SP / 15 wt% CMC. Two colors (black and red) are used to show different regions in the first cycle; b) CV curves of the β–FeOOH. Scanning rate: 0.2 mV s^{-1}

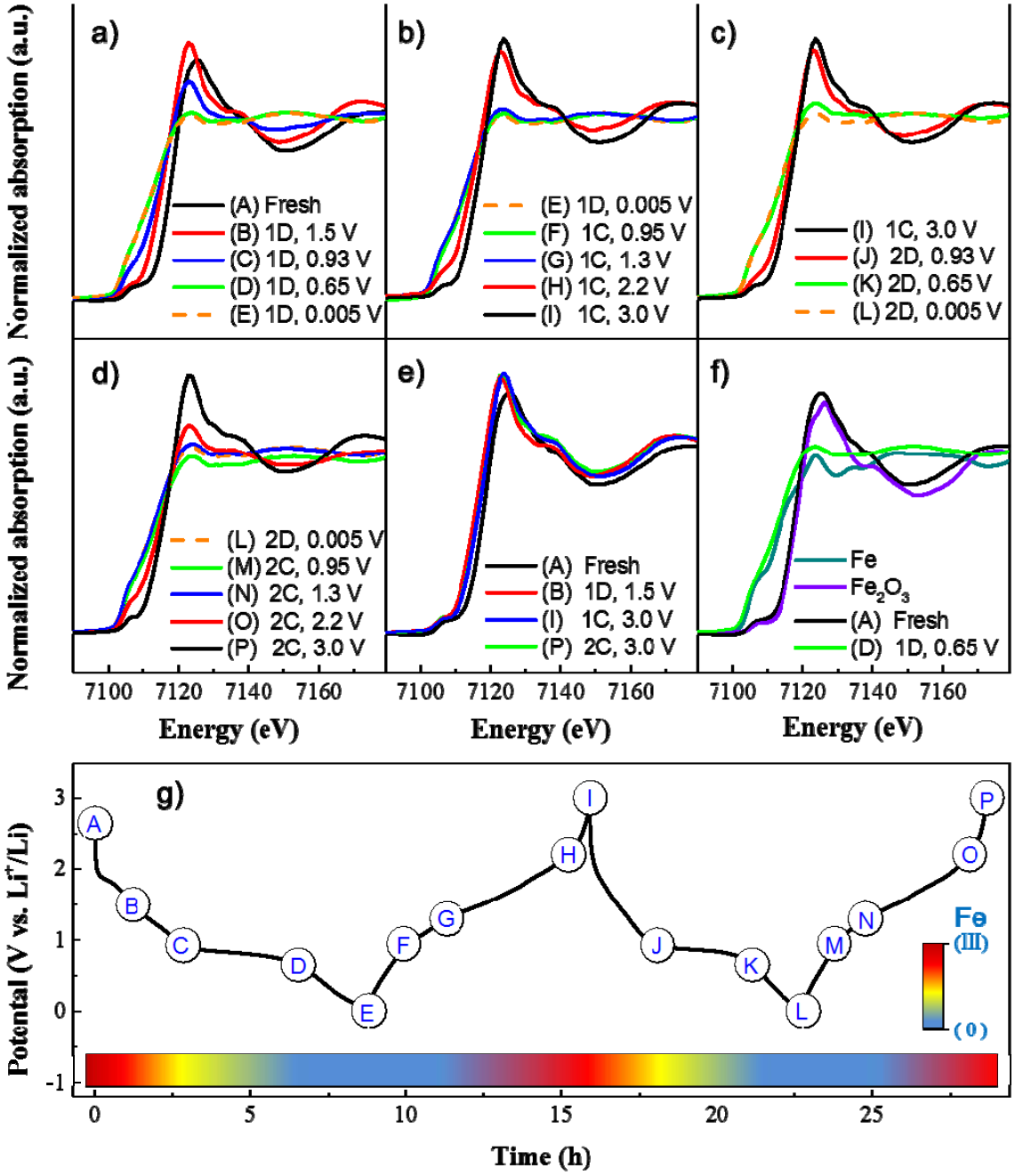

Figure 3. Fe K-edge XANES spectra for β–FeOOH at different lithiation states. a) Fresh electrode and electrodes after the first discharge to 1.5, 0.93, 0.65, and 0.005 V; b) electrodes after the first discharge to 0.005 V and after the first charge to 0.95, 1.3, 2.2, and 3 V; c) electrodes after the first charge to 3 V and after the second discharge to 0.93, 0.65, and 0.005 V; d) electrodes after the second discharge to 0.005 V and after the second charge to 0.95 , 1.3, 2.2, and 3 V; e) fresh electrode and electrodes after the first discharge to 1.5 V, after the first charge to 1 V, and after the second discharge to 3 V. f) fresh electrode, electrode after the first

discharge to 0.65, metallic Fe and Fe_2O_3 references. 1D, 1 C, 2 D, and 2 C in the legends stand for 1st discharge, 1st charge, 2nd discharge, and 2nd charge, respectively. g) Points chosen for XANES study. Approximate valence states of iron during lithiation/delithiation are indicated according to the electrochemcal and XANES results.

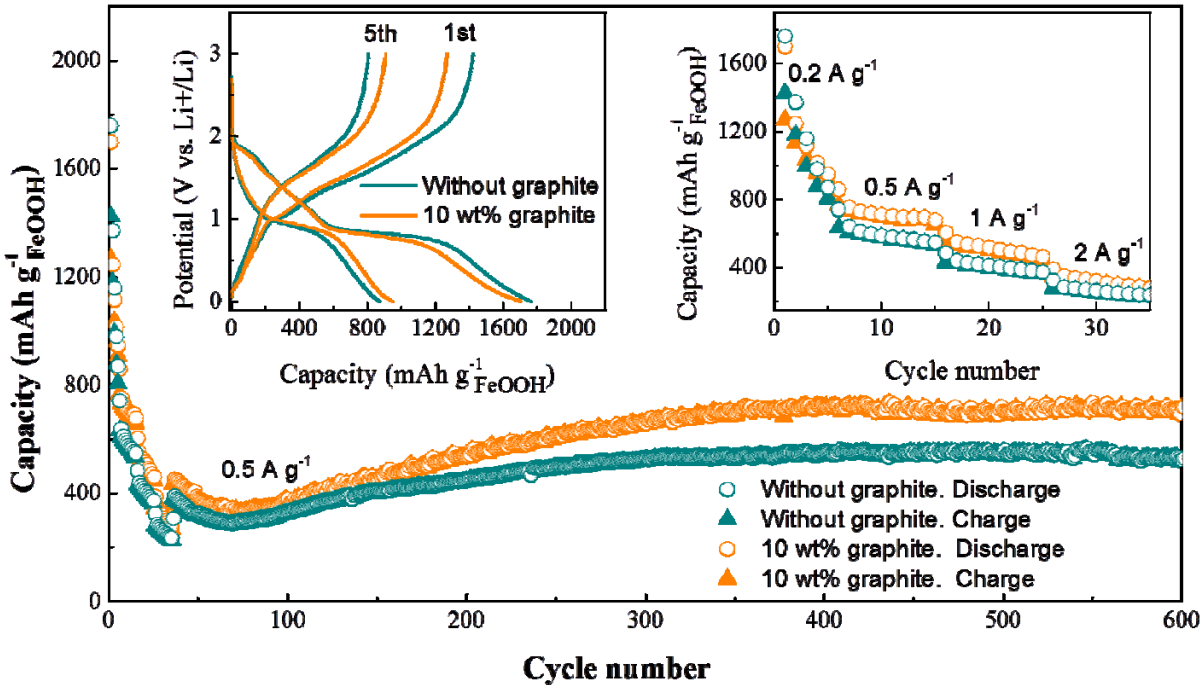

Figure 4. a) Rate and cycling properties of the β–FeOOH. Electrode components for the one without graphite: 70 wt% β–FeOOH-0 / 15 wt% SP / 15wt% CMC; for the one with 10 wt% graphite: 70 wt% β-FeOOH-0 / 10 wt% graphite /5 wt% SP / 15wt% CMC. Current densities (A g^{-1}) applied: 0.2 (1 – 5th cycle), 0.5 (6 – 15th cycle), 1 (16 – 25th cycle), 2 (26 – 35th cycle), and 0.5 (36 – 650th cycle). Inserts show the first and fifth discharge/charge curves (left) and the initial 35 cycles (right)

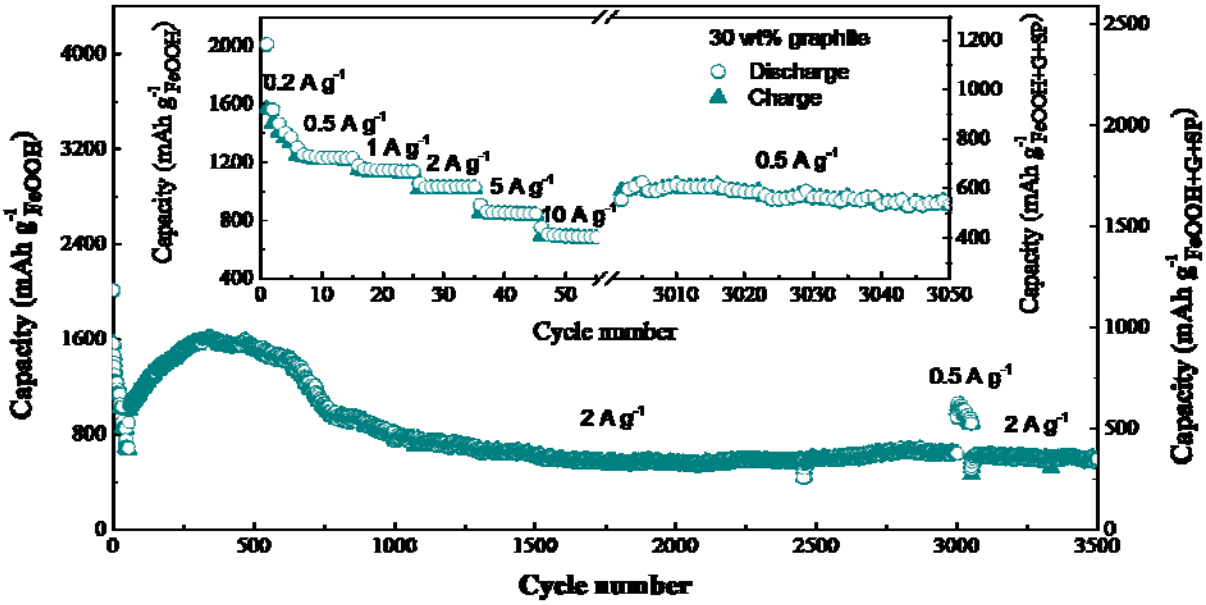

Figure 5. Rate and cycling properties of the β–FeOOH with a high content of graphite. Electrode components: 50 wt% β–FeOOH / 30 wt% graphite / 5 wt% SP / 15 wt% CMC. Current densities (A g^{-1}) applied: 0.2 (1 – 5th cycle), 0.5 (6 – 15th cycle), 1 (16 – 25th cycle), 2 (26 – 35th cycle), 5 (36 – 45th cycle), 10 (46 – 55th cycle), 2 (56 – 3000th cycle), 0.5 (3001 – 3050th cycle), and 2 (the following cycles). Insert shows the cycles 1 – 55th and 3001 – 3050th

The table of contents entry should be 50–60 words long, and the first phrase should be bold.

β–FeOOH is reported to have a very high capacity of ~1400 mAh g^{-1}as an anode for lithium-ion batteries. The storage mechanisms are investigated by a combination of electrochemical and X-ray absorption near edge spectroscopic studies. Very long cycling performance is achieved by a simple electrode design, that even after 3000 cycles the material still has a significant capacity.

Keyword

Linghui Yu, Shibo Xi, Chao Wei, Wenyu Zhang, Yonghua Du,* Qingyu Yan and Zhichuan J. Xu*

Superior Lithium Storage Properties of β–FeOOH